IEEE Photonics Journal
An IEEE Photonics Society Publication

Open Access

Optical Interaction of a Pair of Nanoholes in Au Film via Surface Plasmon Polaritons

Volume 6, Number 3, June 2014

M. Janipour
T. Pakizeh
F. Hodjat-Kashani

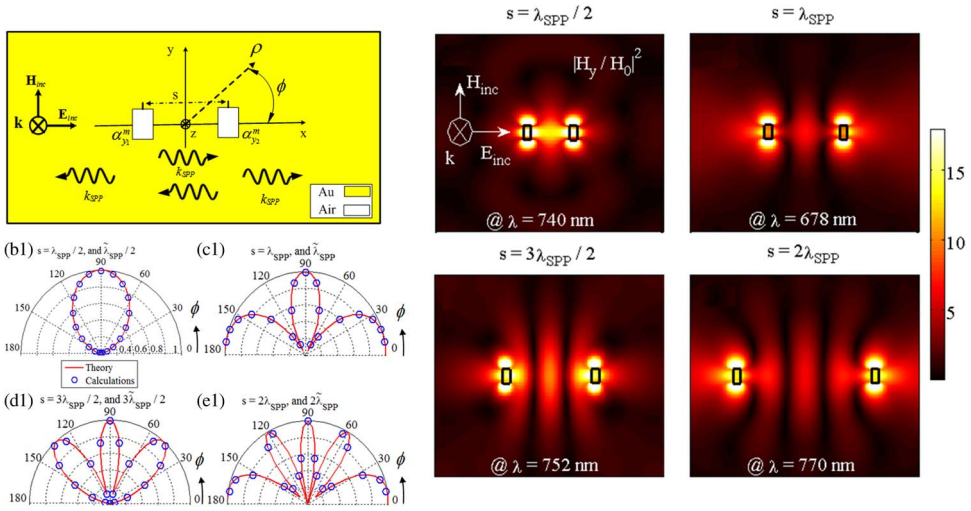

DOI: 10.1109/JPHOT.2014.2326653
1943-0655 © 2014 IEEE

IEEE photonics SOCIETY

IEEE

Optical Interaction of a Pair of Nanoholes in Au Film via Surface Plasmon Polaritons

M. Janipour,[1] T. Pakizeh,[2] and F. Hodjat-Kashani[1]

[1]Department of Electrical Engineering, Iran University of Science and Technology, Tehran 1684613114, Iran
[2]Faculty of Electrical and Computer Engineering, K.N. Toosi University of Technology, Tehran 1631714191, Iran

DOI: 10.1109/JPHOT.2014.2326653

Manuscript received March 20, 2014; revised May 5, 2014; accepted May 7, 2014. Date of publication May 23, 2014; date of current version June 9, 2014. Corresponding author: M. Janipour (e-mail: m_janipour@elec.iust.ac.ir).

Abstract: The optical interaction mechanism of a nanohole pair milled in an opaque gold film by means of surface plasmon polaritons (SPPs) propagation is investigated. This interaction depends on the polarization direction of the incident light and the separation distance between the nanoholes. It is found that when the nanoholes are illuminated by a plane wave incident light polarized parallel to the axis of the nanohole pair, the SPP waves can propagate between the nanoholes, and therefore, the nanoholes can interact through SPPs. In contrast, it is shown that for the incident plane wave polarized perpendicular to the pair axis, the propagation direction of the SPPs is normal to the pair axis, and thus, a weak interaction through the SPPs can occur between the nanoholes. It is also shown that in order to investigate the interaction of the nanoholes through the SPP waves, each nanohole can be modeled by a magnetic dipole, which propagates SPPs. Thus, the optical properties of the interacting nanoholes can be modeled using a magnetic-coupled dipole approximation method accounting SPPs to confirm the simulation results.

Index Terms: Subwavelength structures, plasmonics, surface, nanostructures.

1. Introduction

After exploration of extraordinary optical transmission (EOT) of light through subwavelength apertures milled in a metal film, the attention of researchers have been attracted to the optical features of nanoholes and metallic nanostructures [1]–[4]. The main optical feature of the metallic nanostructures is the ability to circumvent the diffraction limit of the conventional optics [5]. Thus, owing to the collective oscillation of free electrons in noble metals like gold (Au) or silver (Ag), known as plasmons, the photonic devices can be brought into nanoscale [6], [7]. Recent investigations on metallic nanostructures introduced new applications and ideas such as optical metamaterials [8]–[10], nanoantennas [11]–[13], nanobiosensors [14], and nano-spectroscopy [15]. It has been shown that plasmonic waveguides have the potential to manipulate and guide light at deep subwavelength metallic nanostructures. Thus, plasmonics can provide an interface between conventional optics, optoelectronic, and subwavelength devices. One of the most attractive branches of plasmonics is the interaction mechanism between the subwavelength structures exposed by a polarized incident light [16]. It is believed that among these structures a single nanohole or nanohole arrays demonstrate unique features. It has been shown that the localized surface plasmon resonances (LSPR) and their coupling effects with the surface plasmon polaritons (SPPs) play the main role in

the EOT of the subwavelength apertures milled in a noble metal film [17]. Moreover, it is reported that the LSPR of a single nanohole strongly depends on the incident light polarization, the geometry of the nanohole, the material, and the dielectric medium around nanohole and the metallic film [17], [18]. The LSPR of a single nanohole is coupled to the SPP propagation, based on the polarization direction of the incident field [17]. Additionally, it is found that two nanoholes can interact through the propagating SPPs depending on the distance between the nanoholes [18]. Furthermore, it has been shown that a linear chain of the optically coupled nanoholes can treat as a linear wire antenna [19]. There, the coupled nanoholes in a linear chain were analyzed based on electric dipoles [19]–[21]. More recently, it is illustrated that electromagnetic or optical properties of a plasmonic nanohole can be modeled by a resonant magnetic dipole [22]. By placing two nanoholes close by, in the near-field region, they may strongly interact depending on the incident light polarizations. By highlighting the magnetic-field role, the strong optical interaction of the pair of nanoholes is investigated using the introduced magnetic-coupled dipole approximation (MCDA) method in which the magnetic dipoles are coupled through their space-waves in the near-field regime [22].

The present study deals with the optical interaction of a nanohole pair milled in an opaque Au film and situated optically far from each other. The nanoholes are successfully modeled by two tiny magnetic dipoles which are electromagnetically coupled via the propagating SPPs on the surface of the Au film. Thus, instead of the space-wave, the surface-wave is acting as the optical coupling channel of the LSPRs excited in the nanoholes. Therefore, a nanohole might electromagnetically interact with its counterpart even in the intermediate- and far-field regions. Here, the optical properties of the nanostructure are modeled using the MCDA method extended by incorporating the SPPs, called MCDA-SPP. Finally, it is shown that the interference of the excited SPPs via the nanoholes leads to directional propagation of such optical surface-wave, strongly depending on the separation distances between the nanoholes and the polarization of the incident light.

2. Theory and Methods

The known Bethe's principle basically expresses that a single subwavelength aperture milled in a perfect electric conductor (PEC) screen can be modeled using induced parallel magnetic and normal electric dipoles, proportional to the polarization of the incident wave [23]–[25]. In the nanoscale regime, it has been shown that milling a nanohole in a metallic film can be employed to transform the optical energy of the incident light to the SPPs which is due to the established local perturbation on the smooth metal surface [17]. Typically, the SPP waves on the metal-dielectric interface can be lunched using a nanohole [18], [26]–[28]. In this context, it has been found that a dipolar LSPR mode, depending on the geometry and dielectric medium as well as the polarization of the incident light, can be assigned to a nanohole resonance which may be used to lunch the propagating SPPs on a metal surface [17]. Thus, due to the coupling of the LSPR to the SPP waves, the optical intensity propagating on the metal-dielectric interface should exhibit the optical trends similar to that demonstrated by the normalized transmission spectrum.

A nanohole in a metallic film can be adequately modeled by a magnetic dipole in line with the direction of the incident magnetic field [22]. Because of the small size of a nanohole relative to the incident light wavelength, the optical properties of a single nanohole can be analytically determined using the quasi-static approximation method [19], [20]. In addition, it is shown that the magnetic polarizability of a single nanohole can be determined using its relevant electric polarizability [22]. Hence, in order to obtain the magnetic polarizability of the single nanohole at each polarization direction of the incident field, i.e., $\alpha_y^m(\omega)$ and $\alpha_x^m(\omega)$, the proportional electric polarizability should be determined [22], [26], [29], [30]. For instance, an optical plane-wave with $\mathbf{E}^{inc} = E_0\mathbf{a}_x$ which normally illuminates the single rectangular nanohole, milled in an Au-film, is considered. Accordingly, the equivalent magnetization of a single rectangular nanohole can be written as [22], [30]

$$\mathbf{M} = \alpha_y^m(\omega)\mathbf{H}^{\text{inc}} \tag{1}$$

where ω is the angular frequency of the incident wave, $\mathbf{H}^{inc}$ is the incident magnetic field, and $\alpha_y^m(\omega)$ is the magnetic polarizability of the considered nanohole which depends on the permittivity of the metallic film, the dielectric material filled in the nanohole region, the LSPR wavelength (λ_{LSPR}) of the nanohole [22]–[26].

2.1. Theoretical Method: MCDA-SPP

The MCDA method can be used to study the interaction of two or more nanoholes in the near-field regime [22]. Primarily, the introduced MCDA method is successfully employed to theoretically describe the strong optical interaction of two nanoholes positioned in the near-field region of each other [22], without considering any surface wave. Here, the model is extended to investigate the optical interaction of two nanoholes, in the same configuration but positioned optically far from each other, via their SPPs propagating with wavelength λ_{SPP} on a gold film. The present investigation mainly deals with the modality of the optical interaction of two nanoholes separated with the optically long separation distance, namely $s = \lambda_{SPP}/2$, λ_{SPP}, $3\lambda_{SPP}/2$, and $2\lambda_{SPP}$ (i.e., $m\lambda_{SPP}/2$, $m = 1, 2, 3, \ldots$).

Considering an x-polarized incident light (E_x and H_y), a magnetic polarizability in line with the incident magnetic field, i.e., M_y, can be assigned to the single nanohole [see Fig. 2(a)]. The induced magnetic polarizability is directly defined based on the excited LSPR in the nanohole, consequently, the peak position of the normalized optical transmission spectrum through the nanohole can be used to determine λ_{LSPR} of the nanohole.

Since the considered nanoholes are optically small, the asymptotic equations may be used to approximately determine the electric and magnetic fields of the excited SPP by calculating the SPP wave-number k_{SPP}. For a circular nanohole, the field components are theoretically expressed based on the Hankel functions [28]. In fact, a single nanohole with an arbitrary geometrical shape can be used for exciting the SPPs on the surface of a metallic film. Due to the propagation properties of the SPP waves on the metal-dielectric interface, their propagation can be modeled using the cylindrical Hankel functions. Moreover, the propagation wavelength of the SPPs can be determined using k_{SPP} which is coupled to the LSPR wavelength of the nanohole [17]. Thus, the propagation properties of the SPP waves related to the rectangular shaped nanohole can be approximated using the Hankel functions at the proportional LSPR wavelength of the nanohole. Applying the Maxwell's equations in cylindrical coordinate (ρ, φ, z) as defined in Fig. 2(a), the magnetic field of the SPP wave, H_ρ^{SPP}, is expressed in

$$H_\rho^{SPP}(\rho) = \frac{1}{i\omega\mu_0\rho} H_1^{(1)}(k_{SPP}\rho)\cos(\varphi) e^{-\rho/\Gamma}\mathbf{a}_\rho \tag{2}$$

where $k_{SPP} = 2\pi/\lambda_{SPP} + i/\Gamma$ [19], $H_1^{(1)}(k_{SPP}\rho)$ is the Hankel function of first kind and first order, φ is the deviation from x-axis in the xy-plane, ρ is the distance from the origin in the cylindrical coordinate, and the exponential term represents the decay factor in which $\Gamma = 1/(\mathrm{Im}[k_{SPP}])$ is the decay length of the field of the SPP waves [6], [18]. Considering the SPP dispersion relation as $k_{SPP} = k_0\sqrt{\varepsilon_m/(\varepsilon_m + 1)}$, the SPP wavelength (λ_{SPP}) can be theoretically obtained using $\lambda_{SPP} \approx \lambda_0\sqrt{(\mathrm{Re}[\varepsilon_m] + 1)/\mathrm{Re}[\varepsilon_m]} = 670$ nm, at $\lambda_0 = 720$ nm in which $\varepsilon_m = -14.59 + i2.54$ and so the decay constant can be computed as $\Gamma \approx 1090$ nm [27].

In the next step, the optical interaction circumstance between the two nanoholes, in a pair configuration and separated far from each other, can be understood by extending the MCDA method, used to address the strong optical interaction of two nanoholes in near-field region [22]. The extending procedure takes into account the SPP wave of a nanohole which reaches to the other nanohole, thereby it remarkably affects on the local field seen by the nanohole. To perform this, the magnetic field associated to the lunched SPP which is originated from each nanohole or its equivalent magnetic dipole, for the y- and x-polarized incident light, should be considered. These excited fields can be expressed as

$$\begin{Bmatrix} H_{x_j} \\ H_{y_j} \end{Bmatrix} = \begin{Bmatrix} M^x \\ M^y \end{Bmatrix} \left[\frac{1}{i\omega\mu_0\rho} H_1^{(1)}(k_{SPP}\rho) e^{-\rho/\Gamma} \begin{Bmatrix} \sin\varphi \\ \cos\varphi \end{Bmatrix} \right] \tag{3}$$

where $j = 1$ and 2, $M^x = M_1^x = M_2^x$ and $M^y = M_1^y = M_2^y$ are the magnetic polarization of the nanoholes 1 and 2 upon normal incidence of the y- and x-polarized light, respectively. Inserting Eq. (3) in Eq. (1), the modified magnetic polarizabilities of the nanoholes-1 and 2 $(\tilde{\alpha}_{1,2}^m)$ can be obtained. Obviously, they severely depend on the polarization and the separation distance of the two nanoholes. If the incident magnetic field is along the x-axis (or y-polarized light), the modified magnetic polarizability of each nanohole is easily obtained using Eq. (3). Since in this case no magnetic field reaches to other nanohole, $H_{x_i} = 0$ for $\varphi = 0$, for any of the considered separation distance $s = \lambda_{SPP}/2$, λ_{SPP}, $3\lambda_{SPP}/2$, and $2\lambda_{SPP}$, the nanoholes act like isolated single nanoholes, therefore $\tilde{\alpha}_{x_j}^m(\omega) = \alpha_x^m(\omega)$, where $\alpha_{x_1}^m(\omega) = \alpha_{x_2}^m(\omega) = \alpha_x^m(\omega)$. In brief, the optical properties of the nanoholes pair follow trends of that of a single nanohole.

Although, if the incident magnetic field is along y-axis (or x-polarized light) the optical interaction via the SPP waves leads to the modified magnetic polarizabilities as follow:

$$\tilde{\alpha}_{y_j}^m(\omega) = \alpha_y^m(\omega)\left\{\frac{\omega\mu_0 s}{\omega\mu_0 s + i\alpha_y^m(\omega)H_1^{(1)}(k_{SPP}s)e^{-s/\Gamma}}\right\} \tag{4}$$

where $\alpha_{y1}^m(\omega) = \alpha_{y2}^m(\omega) = \alpha_y^m(\omega)$. Equation (4) states that when the nanohole pair is excited by an x-polarized incident light, the nanoholes interact via SPPs in the intermediate- and far-field regions. It should be emphasized that although the LSPR of a single nanohole depends on the geometrical shape of the nanohole, the propagation of the SPPs at the metal-insulator interface can be well approximated using the Hankel functions. Thus, as expressed in Eq. (2), the SPP wave excited by a circular or rectangular nanohole resembles the radiation by a magnetic dipole.

2.2. Computational Method: FDTD

Throughout this paper, the full-wave simulations are performed using the three dimensional finite-difference time-domain (FDTD) method [31], with a spatial unit cell which is determined using uniform discretization with $\Delta x = \Delta y = \Delta z = 5$ nm and without applying any mesh refinement method. In this case, the proper value for time-step (Δt) is determined using Courant–Friedrichs–Lewy (CFL) stability condition using the criterion $\Delta t \leq 1/(c\sqrt{(1/(\Delta x)^2) + (1/(\Delta y)^2) + (1/(\Delta z)^2)})$, where in the case of our problem (i.e., $\Delta x = \Delta y = \Delta z$) simplifies to $\Delta t \leq \Delta x/(c\sqrt{3})$ [31]. The FDTD simulations were performed using a three dimensional MATLAB code on a P4, Intel(R) Core(TM) i7-2630QM CPU 2.00 GHz with 8 GB RAM computer with 64-bit operating system. It is considered that the gold film with dimensions $2500 \times 2500 \times 100$ nm^3 is truncated by convolutional perfectly matched layers (CPMLs) with 32 layers to simulate the required absorbing boundary condition (ABC) [16]. In addition, a total field/scattered field (TFSF) region is considered around computation region containing the nanohole and the Au film in the FDTD method [31]. The TFSF region prevents the interference of the incident plane wave fields with the scattered fields of the nanohole and the gold film in the SF region and hence, produces more accurate results. Figs. 1(a) and (b) demonstrate the simulation layout used in this paper in xy-, and xz-cross sections, respectively.

For the computational purposes, the frequency-dependent dielectric function of Au-film at optical wavelengths is modeled using the Drude-Lorentz (DL) classical model with five poles [30], [32]. The applied DL-model not only accounts for the free-electrons contributions, but also takes into account the interband transitions [32]. The incident plane-wave is considered in the form of an optical Gaussian pulse polarized along x-, and y-axis, respectively [31]. In these simulations, the required time for producing the results is about 10 hours.

3. Results and Discussions

3.1. Single Nanohole

The schematic representation of a rectangular nanohole, with $a = 100$ and $b = 200$ nm, milled in a gold film with thickness $d = 100$ nm, is shown in Fig. 2(a). In the quasi-static limit, the depolarization

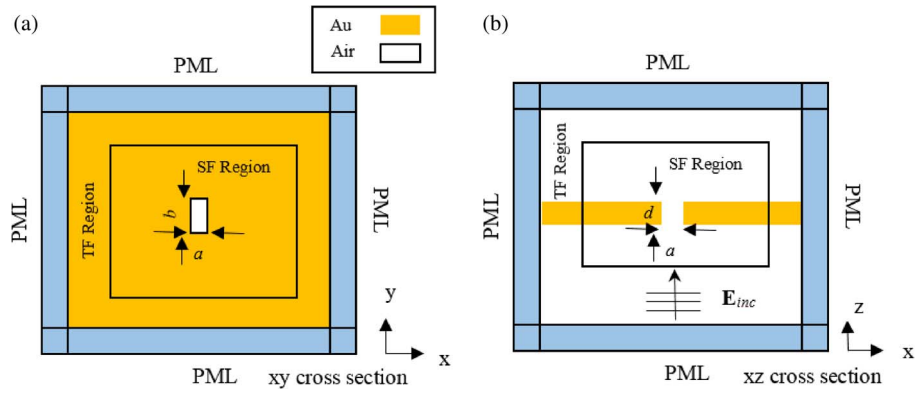

Fig. 1. (a) The layout of the simulation region in (a) *xy* cross section and (b) *xz* cross section.

factors for the *x*-polarized incident light (i.e., α_x^e and α_y^m) with wavenumber $k_0 = 2\pi/\lambda_0$ can be obtained as [22], [30]

$$\begin{cases} L_x = \frac{2}{\pi}\tan^{-1}\frac{bd}{a\sqrt{a^2+b^2+d^2}} \\ L_y = \frac{2}{\pi}\tan^{-1}\frac{da}{b\sqrt{a^2+b^2+d^2}} \\ L_z = \frac{2}{\pi}\tan^{-1}\frac{ab}{d\sqrt{a^2+b^2+d^2}} \end{cases} \tag{5}$$

These depolarization factors are used to obtain the electric polarizability of the nanohole which can be computed using a special case of the Clausius-Mossotti relation in the form of $\alpha_x^e \propto [\varepsilon_{air} - \varepsilon_{Au}]/[(1 - L_x)\varepsilon_{Au} + L_x\varepsilon_{air}]$, [26]. The magnetic polarizability is achieved based on $\alpha_y^m \approx -i[M - Nk_0^2]/[M - Nkk_0]\alpha_x^e$, where $M = kk_x\omega\varepsilon_0$, $N = \sqrt{\varepsilon_0/\mu_0}(k_y^2/k_x)$, $k_x = i\pi/(a + 2\delta)$, $k_y = \pi/(b + 2\delta)$, and $k = \sqrt{k_y^2 - k_y^2}$ [22]. In these equations δ is the skin depth of the gold film [14]. Similarly the depolarization factors can be found for the *y*-polarized incident light (i.e., α_y^e and α_x^m) by rotating the rectangle or switching *a* with *b* in Eq. (5). As shown in Fig. 2(a), assuming point-A on the *xy*-plane and above the gold film at $z = 10$ nm, one can evaluate the spectrum of the optical intensity reached to the considered point. It is expected that the propagated optical intensity spectrum to an arbitrary point on the surface far from the nanohole, mediated by the SPPs should exhibit the spectral properties like the optical transmission spectrum. It should be noted that, in this study it is considered that the incident wave normally illuminates the gold film.

Fig. 2(b) shows the normalized optical intensity at point A (solid-line) in comparison with the normalized optical transmission spectrum of the nanostructure (dashed-line). According to Fig. 2(b), it can be seen that the spectral peak position of the calculated intensity at an arbitrary point along the polarization of the incident field, e.g., point-A, is coincide with the observed peak position in the transmission spectrum. More importantly, it is seen that the LSPR of the single nanohole is coupled to the propagating SPP waves on the metal surface. Expectedly, the SPP's radiated power at the λ_{LSPR} of the nanohole is stronger than the other wavelengths in the interested spectrum. Fig. 2(c) shows the simulated normalized intensity of the induced magnetic field $(|H_y/H_0|^2)$ on the surface of the nanostructure shown in Fig. 2(a), at $\lambda = 720$ nm. Essentially, as can be seen in Fig. 2(c), the fields around the nanohole in the near-field region illustrate a magnetic dipolar nature. However, as one goes further far from the nanohole, the fields propagate on the metal surface in the form of SPP waves. The far-field radiation or propagation $(\mathbf{E} \times \mathbf{H}^*)$ pattern of the SPP in the azimuth $(\varphi-)$ plane for the single nanohole which obeys $\cos^2(\varphi)$ [33]–[35], unlike the radiation pattern of an electric dipole which follows $\sin^2(\varphi)$ [12], is shown in Fig. 2(e). There, the far-field radiation pattern of the SPP, lunched by the nanohole, is obtained using the theory (solid-line, based on [33]–[35]) and the FDTD calculations (circles), at $\lambda = 720$ nm. It can be clearly seen

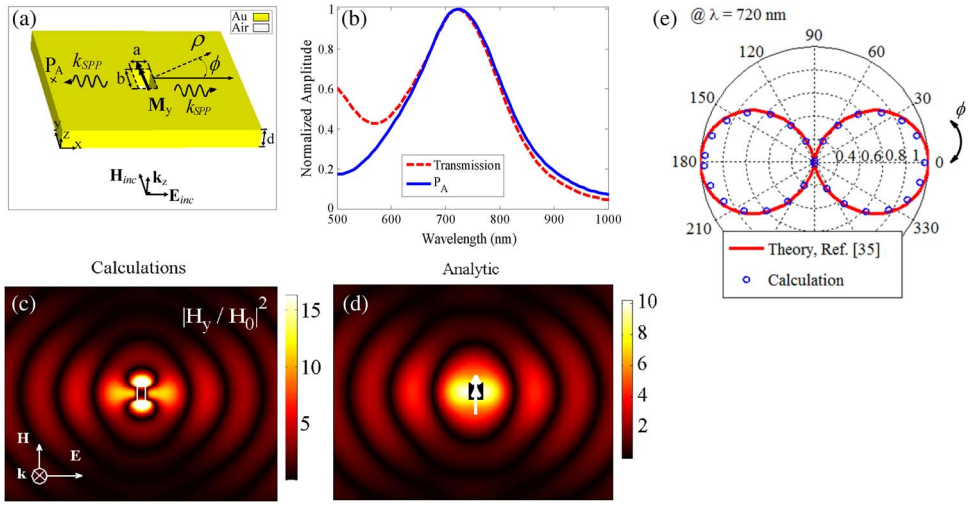

Fig. 2. (a) The schematic representation of the induced magnetic dipole (M_y) in a rectangular nanohole ($a \times b$), milled in an Au film with thickness d. (b) The calculated optical intensity at point-A (solid line) compared to the normalized transmission (red dashed line) of the nanohole. Intensity distributions of the induced magnetic field ($|H_y/H_0|^2$) of the SPP excited by the nanohole with $a = 100$, $b = 200$ nm, and thickness $d = 100$ nm using (c) calculations and (d) analytic method (see (2)), at $\lambda = 720$ nm. (d) The far-field azimuth (phi) propagation pattern of the SPP lunched by the single nanohole using the calculations (circles) and the theory (red solid-line, based on [35]), at $\lambda = 720$ nm.

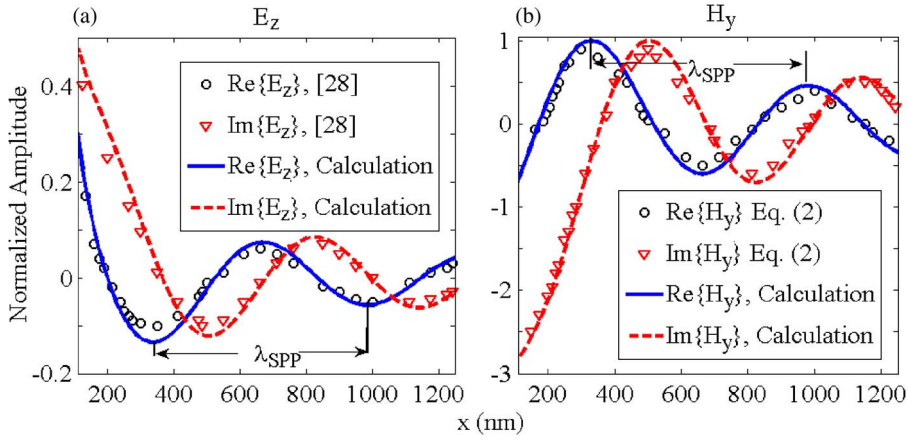

Fig. 3. Normalized amplitudes of the (a) real (solid-line) and imaginary (dashed-line) parts of the calculated induced magnetic field, H_y component, of the propagated SPPs of the rectangular nanohole (shown in Fig. 2(a)) along x-axis at $\lambda = 720$ nm (λ_{LSPR}) in comparison with the real (circles) and imaginary (triangles) parts obtained using Eq. (2). (b) The real (solid-line) and imaginary (dashed-line) parts of the calculated E_z, compared with real (circles) and imaginary (triangles) parts of $E_z$of the SPPs at λ_{LSPR}, adapted from Ref. [28].

that the nanohole excites the SPP, propagating on the metal surface similar to the magnetic dipole radiation.

Fig. 3(a) shows the normalized amplitude of the real (solid-line), and imaginary (dashed-line) parts of the calculated H_y of the SPP wave versus x-axis compared with the real (circles) and imaginary (triangles) parts of the induced magnetic field of the SPP wave using Eq. (2) for the rectangular nanohole shown in Fig. 2(a). Similarly, Fig. 3(b) shows the normalized amplitude of the real (solid-line) and imaginary (dashed-line) parts of the calculated E_z field of the SPP lunched by the rectangular shaped nanohole along x-axis at $\lambda_{LSPR} = 720$ nm, in comparison with the real

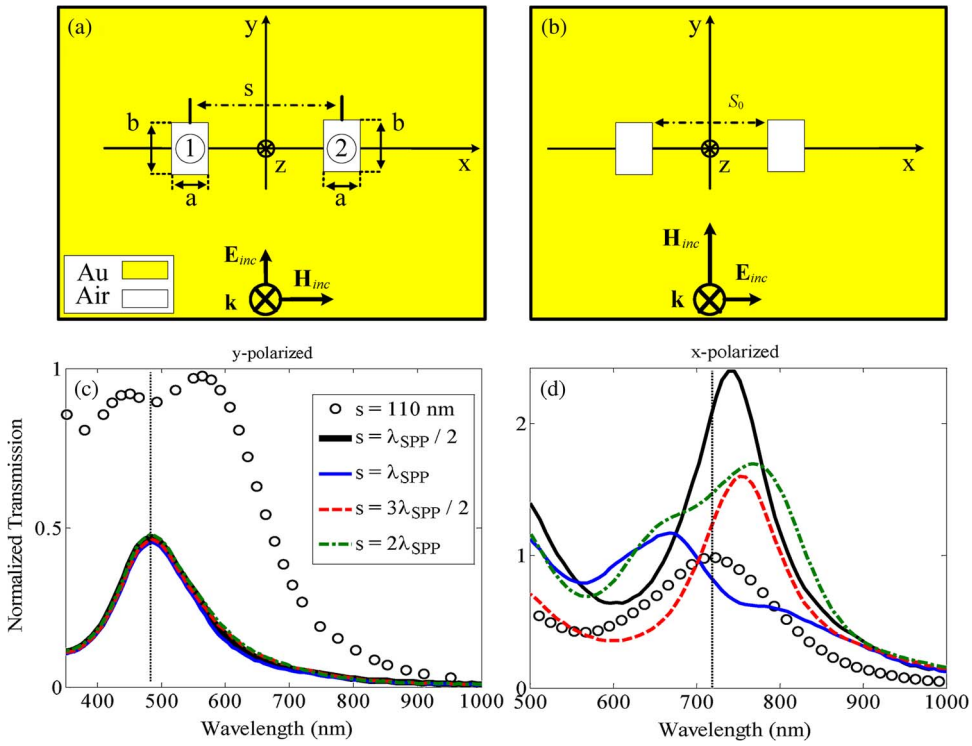

Fig. 4. The configuration geometry of the nanohole pair for the (a) *y*-polarized and (b) *x*-polarized incident plane-wave. The normalized transmission of the nanostructure, with $a = 100$, $b = 200$, and $d = 100$ nm, for the y-polarized (c) and *x*-polarized (d) illuminations versus separation distances $s = 110$ nm (circles), $\lambda_{SPP}/2$ (thick solid-line), λ_{SPP} (solid-line), $3\lambda_{SPP}/2$ (dashed-line), and $2\lambda_{SPP}$ (dash-dotted line). The vertical dotted-lines denote the transmission of the gold film due to the intraband transition for the *y*-polarized incident field, and the LSPR-wavelength of the single nanohole for the *x*-polarized incident field.

(circles) and imaginary (triangles) parts of E_z field adapted from Ref. [28]. Certainly, the calculations nicely support the theory and the reported data. As can be seen in Figs. 3(a) and (b), the electric and magnetic fields of the SPP wave, excited by the rectangular nanohole, propagating along *x*-axis at λ_{LSPR}, can be well approximated using the Hankel functions, described in Eq. (2). Moreover, as distinguished in Figs. 3(a) and (b), λ_{SPP} can be directly extracted using the maximum peaks or minimum deeps of the electric or magnetic fields, i.e., $\lambda_{SPP} = 680$ nm, which approximately confirms the theoretically obtained value $(\tilde{\lambda}_{SPP} \sim 670 \text{ nm})$.

3.2. Nanohole Pair

The schematic representations of two nanoholes, separated by distance *s*, normally illuminated by a plane-wave light with *y*- and *x*-polarization are shown in Fig. 4(a) and (b), respectively. Fig. 4(c) and (d) show the normalized transmission of the nanoholes pair, shown in Fig. 4(a) and (b), and separated by $s = \lambda_{SPP}/2$ (thick solid-line), λ_{SPP} (solid-line), $3\lambda_{SPP}/2$ (dashed-line), and $2\lambda_{SPP}$ (dash-dotted line), knowing that $\lambda_{SPP} = 680$ nm. The optical transmissions are compared with the transmission of the strongly interacting nanohole pair for which the edge-to-edge separation distance is $s_0 = 10$ nm (circles), i.e., the nanoholes are placed in the near-field region of each other. The vertical dotted lines in Figs. 4(c) and (d) denote the spectral peak positions of the optical transmission associated to the direct transmission of the gold film under the *y*-polarized excitation due to the intraband transition [36], and the excited LSPR of the considered single nanohole under the *x*-polarized excitation, respectively.

In the case of the *y*-polarized incident light, the strong interaction occurs between the nanoholes for distance $s = 110$ nm (or $s_0 = 10$ nm), denoted by circular-dots in Fig. 4(c), and discussed in

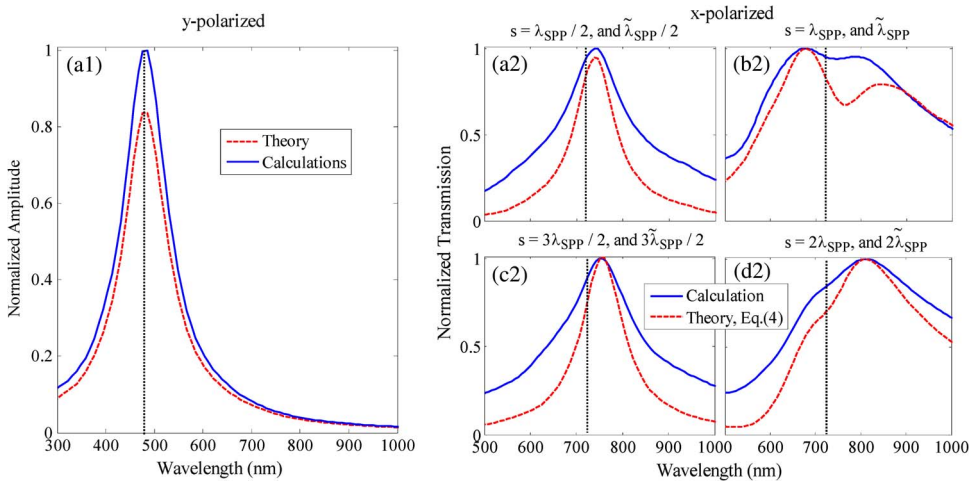

Fig. 5. The normalized near-field amplitude of the induced magnetic field at the center of the nanohole-1 (or 2) and at $z = 10$ nm above the film using the calculations (solid-line), in comparison with the amplitude of the modified magnetic polarizability obtained from the theory (dashed-line), for the y-polarized incident light (a1), and for the x-polarized incident light (right-column) while the distance $s = \lambda_{SPP}/2$, and $\tilde{\lambda}_{SPP}/2$ (a2), λ_{SPP}, and $\tilde{\lambda}_{SPP}$ (b2), $3\lambda_{SPP}/2$, and $3\tilde{\lambda}_{SPP}/2$ (c2), $2\lambda_{SPP}$ and $2\tilde{\lambda}_{SPP}$ (d2). The vertical dotted-lines denote of λ_{LSPR} the single nanohole.

[22]. By increasing the separation distance, the interaction vanishes gradually and thus, a single resonant peak remains in the transmission spectrum for longer separation distances. More precisely, for $s = \lambda_{SPP}/2$, λ_{SPP}, $3\lambda_{SPP}/2$, and $2\lambda_{SPP}$ a single resonant peak, at λ_{LSPR}, is seen in the optical transmission spectrum. Expectedly, the peak position of the optical transmission of a single nanohole is indeed at λ_{LSPR}, denoted by the vertical dotted-line in Fig. 4(c). There, the optical properties of the pair with different s, exposed by the y-polarized incident field, follow similar trends. This feature is due to the fact that the SPP propagation direction is in consonance with the incident electric field polarization direction. Thus, it can be inferred that for the polarization perpendicular to the nanohole pair axis, the coupling between the nanoholes for $s \geq \lambda_{SPP}/2$ is very weak.

In contrast, the optical transmission of the nanohole pair, illuminated by x-polarized incident light, exhibit starkly different distant-dependent features. According to Fig. 4(d), for $s = 110$ nm (near-field region) or $s_0 = 10$ nm, it is discernible that the nanohole pair resonates at the wavelength which is close to λ_{LSPR} of the single nanohole (vertical dotted-line), or two non-interacting nanoholes. In fact, for this arrangement of nanohole pair, excited by the x-polarized incident wave, the near-field optical interaction of the nanoholes is negligible [22]. Although, as it can be seen from Fig. 4(d) that for the case of $s = \lambda_{SPP}$ and $2\lambda_{SPP}$ two resonant peaks are obvious in the transmission spectrum; while for the case of $s = \lambda_{SPP}/2$, and $3\lambda_{SPP}/2$ the transmission is enhanced and its spectrum exhibits only one resonant peak. Correspondingly, for long s, if the x-polarized incident light illuminates the nanohole pair, an effective optical interaction may occur between the nanoholes, leading to optical properties which substantially deviate from that of a single nanohole.

The calculated results are compared with the results of the developed theory, the MCDA-SPP method. For this purpose, the magnetic field close to the nanohole are numerically calculated (solid-line) and compared with the theoretical results (dashed-line) obtained based on the modified magnetic polarizabilities of the nanoholes. In the y-polarized incident light case, the corresponding normalized near-field amplitude of the induced magnetic field (H_x) of the nanohole-1 (or nanohole-2) at the center of the nanohole and $z = 10$ nm above the film, is shown in Fig. 5(a1). The spectrum demonstrates a single peak at $\lambda = 485$ nm using the both calculations and the theory.

However, for an x-polarized incident light, the calculated normalized near-field amplitudes of the induced magnetic fields (H_y) which adequately support the theoretical solutions (dashed line),

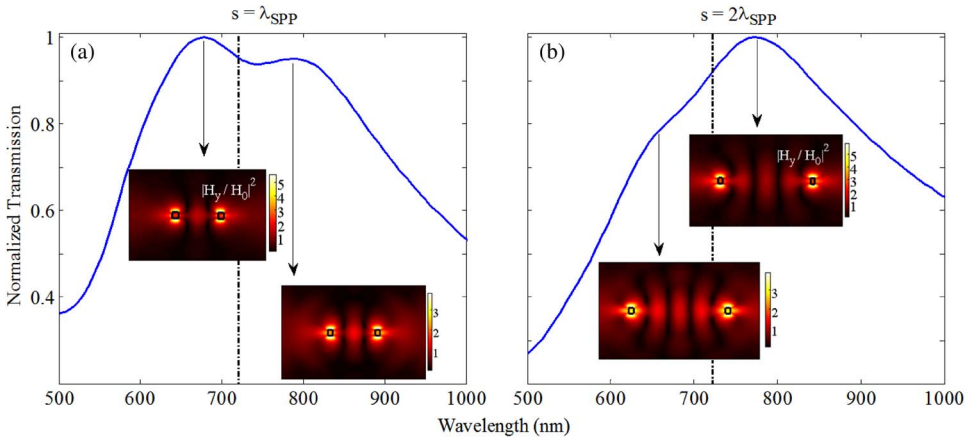

Fig. 6. The normalized transmission through the nanohole pair for distance $s = \lambda_{SPP}$ (a) and $2\lambda_{SPP}$ (b). The vertical dotted-lines denote λ_{LSPR} of the single nanohole. In the insets, the distributions of the induced magnetic field ($|H_y/H_0|^2$), obtained from calculations, are shown at the observed two peak wavelengths.

based on Eq. (4), are shown in the right-column of Fig. 5, for the distance $s = \lambda_{SPP}/2$, $\tilde{\lambda}_{SPP}/2$ (a2), λ_{SPP}, $\tilde{\lambda}_{SPP}$ (b2), $3\lambda_{SPP}/2$, $3\tilde{\lambda}_{SPP}$ (c2), and $2\lambda_{SPP}$, $2\lambda_{SPP}$ (d2) for the calculation and the theory; respectively.

According to Figs. 5(a2) and (c2) it can be seen that the normalized near-field amplitudes for $s = \lambda_{SPP}/2$, $\tilde{\lambda}_{SPP}/2$, and $3\lambda_{SPP}/2$, $3\tilde{\lambda}_{SPP}/2$ demonstrate a single peak at $\lambda = 740$ and 752 nm, respectively; which they are red-shifted relative to the LSPR of the single nanohole (vertical dotted-lines). This is because for the wavelengths below the resonance, the fields due to the induced charges at each nanohole amplify the external fields at the other nanohole and consequently red-shift the peak of the induced magnetic field [36]. However, as can be seen in Fig. 5(b2), for $s = \lambda_{SPP}$, $\tilde{\lambda}_{SPP}$ the both calculation and theory illustrate two resonant peaks in the interested spectrum. These peaks occur because at the wavelengths upper than λ_{LSPR} of the single nanohole, the fields caused by the induced charges at each nanohole decrease the external fields at the other nanohole (so cause a blue-shift) while for the wavelengths lower than λ_{LSPR} enhance the external fields at the other nanohole which in turn rises the red-shift [37]. This situation is reversed for $s = 2\lambda_{SPP}$, $2\tilde{\lambda}_{SPP}$ [Fig. 5(d2)].

In order to elucidate these phenomena, the transmission spectrum of the nanohole pair is separately shown in Figs. 6(a), and 6(b) for $s = \lambda_{SPP}$, and $2\lambda_{SPP}$, respectively. The induced magnetic fields ($|H_y/H_0|^2$) related to the SPP excitations (the insets) and also the optical transmission spectrum of the nanohole pair are shown in Fig. 6(a) at $\lambda = 678$ and 780 nm, and also in the insets of Fig. 6(b) at $\lambda = 660$ and 770 nm, correspondingly. Interestingly, for $s = \lambda_{SPP}$, the intensity at $\lambda = 678$ nm is similar to the intensity at $\lambda = 780$ nm but with a greater intensity. In contrast, the intensity of the induced magnetic field in the inset of Fig. 6(b), for $s = 2\lambda_{SPP}$, shows that the intensity distribution at $\lambda = 660$ nm is also similar to the intensity at $\lambda = 770$ nm but with a reduced intensity.

Attaching to the importance of the separation distance role the optical interaction of the nanoholes, specially when the nanohole pair is illuminated by the *x*-polarized light, the other two distances, i.e., $s = \lambda_{SPP}/2$ and $3\lambda_{SPP}/2$, are considered as well. In this regard, the planar distributions of the calculated normalized intensities of the induced magnetic field ($|H_y/H_0|^2$) for all the considered distances are shown in Fig. 7(a1)–7(d1). These results are compared with the intensities shown in Fig. 7(a2)–7(d2), obtained using the theory [Eq. (3)]. Although it is evident that the theoretical results are in good agreement with the computational results, they fail to illustrate the local dipolar magnetic field around the nanoholes. This is expected since the finite-size rectangular nanoholes are modeled by point magnetic dipoles which are coupled via the SPPs,

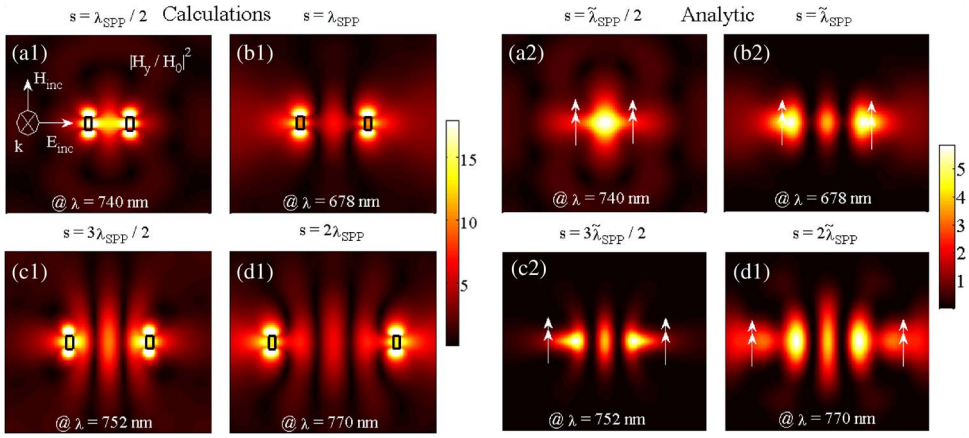

Fig. 7. Distributions of the normalized intensities of the induced magnetic field ($|H_y/H_0|^2$) of the nanohole pair shown in Fig. 4(a) using the numerical calculations (left-column) and the analytical method, Eq. (3), (right-column) for distance $s = \lambda_{SPP}/2$, and $\tilde{\lambda}_{SPP}/2$ (a1,a2) at $\lambda = 740$ nm, $s = \lambda_{SPP}$, and $\tilde{\lambda}_{SPP}$ (b1,b2) at $\lambda = 678$ nm, $s = 3\lambda_{SPP}/2$, and $3\tilde{\lambda}_{SPP}/2$ (c1, c2) at $\lambda = 752$ nm, and $s = 2\lambda_{SPP}$, and $2\tilde{\lambda}_{SPP}$ (d1,d2) at $\lambda = 770$ nm.

and also, the analytic distributions only account for the excited SPPs on the Au surface, originating from dipoles, denoted by the arrows in Fig. 7(a2)–7(d2), and they interfere far from the nanoholes.

For $s = \lambda_{SPP}/2$, $\tilde{\lambda}_{SPP}/2$ according to Fig. 7(a1) and (a2), it can be seen that for the *x*-polarized incident light and at $\lambda = 740$ nm the interaction of the nanoholes via their SPPs leads to the predominant propagation of the SPP waves in $\varphi = \pi/2$ direction. Also, according to Fig. 7(c1) and (c2) for $s = 3\lambda_{SPP}/2$, $3\tilde{\lambda}_{SPP}/2$ at $\lambda = 752$ nm, the interference of the SPP waves generates a higher order mode of the SPP propagation compared to $s = \lambda_{SPP}/2$, $\tilde{\lambda}_{SPP}/2$. In contrast, regarding to Fig. 7(b1) and (b2), for $s = \lambda_{SPP}$, $\tilde{\lambda}_{SPP}$ at $\lambda = 678$ nm the interaction of the nanoholes mediated by SPPs, leads to the efficient SPP propagation along $\varphi = 0$, π, and $\pi/2$ directions. Hence, the manipulation and control of the far-field propagation pattern of the resulting surface wave is possible by tuning the separation distance and the polarization.

The polarization effect on the optical interaction of the nanohole pair via their SPPs is illustrated in Fig. 8. The schematic representations of the events are shown in Fig. 8(a1) and (a2) for the *x*- and *y*-polarized incident light, respectively. Considering the nanohole pair as the in-phase magnetic dipoles which are coupled via the SPP waves [see Fig. 8(a1)], the total radiation or propagation pattern can be written as [38]

$$H = H_1 + H_2 = M\left[e^{ik_{SPP}s/2} + e^{-ik_{SPP}s/2}\right] = M \times \cos\left[\frac{k_{SPP}s}{2}\cos\varphi\right] \tag{6}$$

where $M_1 = M_2 = M$, because of the uniform excitation of the nanohole pair. Equation (6) leads to $H\infty\cos[\pi/2\cos\varphi]$ and $H\infty\cos[3\pi/2\cos\varphi]$ for the case of $s = \tilde{\lambda}_{SPP}/2$, and $3\tilde{\lambda}_{SPP}/2$, respectively. However, for the former case the maximum radiation occurs at $\varphi = \pi/2$, for the latter occurs at $\varphi = \pi/4$, $\pi/2$, and $3\pi/4$. But, $H\infty\cos[\pi\cos\varphi]$ and $H\infty\cos[2\pi\cos\varphi]$ for $s = \tilde{\lambda}_{SPP}$ and $2\tilde{\lambda}_{SPP}$, respectively. Thus, the main lobes of the radiation patterns occur at $\varphi = 0$ and π. In these cases, the side lobes of the radiation patterns are seen at $\varphi = \pi/2$ for $s = \tilde{\lambda}_{SPP}$, and at $\varphi = \pi/3$, $\pi/2$, and $2\pi/3$ for $s = 2\tilde{\lambda}_{SPP}$. Figs. 8(b1)–(e1) show the normalized radiation pattern for $s = \lambda_{SPP}/2$, $\tilde{\lambda}_{SPP}/2$ Fig. 8(b1), λ_{SPP}, $\tilde{\lambda}_{SPP}$ Fig. 8(c1), $3\lambda_{SPP}/2$, $3\tilde{\lambda}_{SPP}/2$ Fig. 8(d1), and $2\lambda_{SPP}$, $2\tilde{\lambda}_{SPP}$ Fig. 8(e1), respectively, which is obtained based on the calculations (circles), and theory (solid line) using Eq. (6) for the *x*-polarized incident light. The same procedure can be applied to the nanostructure shown in Fig. 8(a2). In this case, it is sufficient to multiply Eq. (6) in $\sin\varphi$. The resulting far-field radiation patterns of the nanohole pair illuminated by a *y*-polarized incident light are shown in

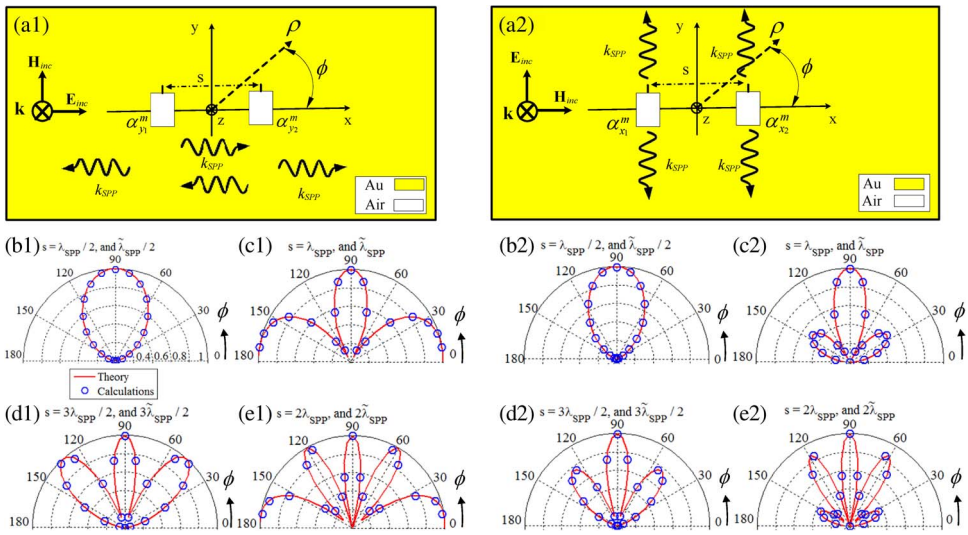

Fig. 8. Directional propagation of the lunched SPPs of the nanohole pair on the gold film. (a1), (a2) Schematic representation of the nanohole pair which is excited by an *x*- and *y*-polarized incident light and the related magnetic dipoles, respectively. The normalized radiation patterns of the nanostructures, in φ -plane, obtained from theory (red solid-line) based on Eq. (6) and the FDTD calculations (circles) for $s = \lambda_{SPP}/2$, $\tilde{\lambda}_{SPP}/2$ [(b1) at $\lambda = 740$ nm, (b2)], $s = \lambda_{SPP}$, $\tilde{\lambda}_{SPP}$ [(c1) at $\lambda = 678nm$, (c2)], $s = 3\lambda_{SPP}/2$, $3\tilde{\lambda}_{SPP}/2$ [(d1) at $\lambda = 752$ nm, (d2)], and $s = 2\lambda_{SPP}$, $\tilde{\lambda}_{SPP}$ [(e1) at $\lambda = 770$ nm, (e2)]. All the patterns in the right-column side (b2–e2) are plotted at $\lambda = 485$ nm.

Figs. 8(b2)–(e2) for $s = \lambda_{SPP}/2$, $\tilde{\lambda}_{SPP}/2$ Fig. 8(b2), λ_{SPP}, $\tilde{\lambda}_{SPP}$ Fig. 8(c2), $3\lambda_{SPP}/2$, $3\tilde{\lambda}_{SPP}/2$ Fig. 8(d2), and $2\lambda_{SPP}$, $2\tilde{\lambda}_{SPP}$ Fig. 8(e2), respectively. Moreover, according to Fig. 8, it can be seen that in fact the radiation patterns for $s = 3\lambda_{SPP}/2$ and $2\lambda_{SPP}$ exhibit the features of the higher order mode SPPs, compared to the radiation patterns for $s = \lambda_{SPP}/2$ and λ_{SPP}. It should be noted that for $s = \lambda_{SPP}$ the radiation pattern of the resulting SPP of the nanohole pair at the first peak-position of the optical transmission (see Fig. 6(a)), i.e., $\lambda = 678$ nm, is similar to the radiation pattern at the second peak-position, i.e.,$\lambda = 780$ nm. Similarly, the radiation pattern for $s = 2\lambda_{SPP}$ at $\lambda = 660$ nm is the same as the observed pattern at $\lambda = 770$ nm.

Apart from the flexibilities and capabilities of the introduced method of tuning and engineering of the SPP propagation on the metal surface by using two interacting nanoholes, the rigorous semi-analytical or numerical calculations such as Green function method and the FDTD method require considerable memory space and run-time. Thus, the proposed simple MCDA-SPP method offer a great potential for faster analyzing, modeling, and calculating of the optical properties of the plasmonic nanoholes arranged in different configurations, paving the way toward more efficient engineering of SPPs using planar plasmonic nanostructures.

4. Conclusion

In conclusion, the optical interaction of two rectangular shaped nanoholes milled in a gold film through SPP propagation is investigated in different polarizations and separation distances under uniform excitation. It is shown that when the incident electric field is polarized along the axis of the nanohole pair, the nanoholes can interact through SPP waves if the nanoholes are positioned in the intermediate/far field region of each other. In addition, the nanoholes have been modeled with magnetic dipoles which propagate SPPs on the metal-dielectric interface depending on the polarization direction of the incident field. The applied MCDA-SPP method to the magnetic dipoles, related to each nanohole, shows that the nanoholes can interact through the SPP waves as two in-phase magnetic dipoles. Thus, the MCDA-SPP method which approximates the calculations very well, can be used to evaluate the interaction of the nanoholes via SPPs.

References

[1] T. W. Ebbesen, H. J. Lezec, H. F. Ghaemi, T. Thio, and P. A. Wolff, "Extraordinary optical transmission through sub-wavelength hole arrays," *Nature*, vol. 391, no. 6668, pp. 667–669, Feb. 1998.

[2] D. E. Grupp, H. J. Lezec, T. Thio, and T. W. Ebbesen, "Beyond the bethe limit: Tunable enhanced light transmission through a single sub-wavelength aperture," *Adv. Mater.*, vol. 11, no. 10, pp. 860–862, Jul. 1999.

[3] A. Degiron and T. W. Ebbesen, "The role of localized surface plasmon modes in the enhanced transmission of periodic subwavelength apertures," *J. Opt. A, Pure Appl. Opt.*, vol. 7, no. 2, pp. S90–S96, Feb. 2005.

[4] J. M. Vigoureux, "Analysis of the Ebbesen experiment in the light of evanescent short range diffraction," *Opt. Commun.*, vol. 198, no. 4–6, pp. 257–263, Nov. 2001.

[5] W. L. Barnes, A. Dereux, and T. W. Ebbesen, "Surface plasmon subwavelength optics," *Nature*, vol. 424, no. 6950, pp. 824–830, Aug. 2003.

[6] L. Novotny and B. Hecht, *Principles of Nano-optics*. Cambridge, U.K.: Cambridge Univ. Press, 2006.

[7] E. Ozbay, "Plasmonics: Merging photonics and electronics at nanoscale dimensions," *Science*, vol. 311, no. 5758, pp. 189–193, Jan. 2006.

[8] J. B. Pendry, "Negative refraction makes a perfect lens," *Phys. Rev. Lett.*, vol. 85, no. 18, pp. 3966–3969, Oct. 2000.

[9] G. Dolling, C. Enkrich, M. Wegener, C. M. Soukoulis, and S. Linden, "Simultaneous negative phase and group velocity of light in a metamaterial," *Science*, vol. 312, no. 5775, pp. 892–894, May 2006.

[10] S. Zhang *et al.,* "Experimental demonstration of near-infrared negative-index metamaterials," *Phys. Rev. Lett.*, vol. 95, no. 13, pp. 137404-1–137404-4, Sep. 2005.

[11] D. P. Fromm, A. Sundaramurthy, P. J. Schuck, G. Kino, and W. E. Moerner, "Gap-dependent optical coupling of single "Bowtie" nanoantennas resonant in the visible," *Nano Lett.*, vol. 4, no. 5, pp. 957–961, May 2004.

[12] T. Pakizeh and M. Käll, "Unidirectional ultracompact optical nanoantennas," *Nano Lett.*, vol. 9, no. 6, pp. 2343–2349, Jun. 2009.

[13] H. J. Lezec *et al.,* "Beaming light from a subwavelength aperture," *Science*, vol. 297, no. 5582, pp. 820–822, Aug. 2002.

[14] T. Rindzevicius *et al.,* "Plasmonic sensing characteristics of single nanometric holes," *Nano Lett.*, vol. 5, no. 11, pp. 2335–2339, Nov. 2005.

[15] H. X. Xu, E. J. Bjerneld, M. Käll, and L. Borjesson, "Spectroscopy of single hemoglobin molecules by surface enhanced Raman scattering," *Phys. Rev. Lett.*, vol. 83, no. 21, pp. 4357–4360, Nov. 1999.

[16] T. Pakizeh, M. S. Abrishamian, N. Granpayeh, A. Dmitriev, and M. Käll, "Magnetic-field enhancement in gold nanosandwiches," *Opt. Exp.*, vol. 14, no. 18, pp. 8240–8246, Sep. 2006.

[17] T. Rindzevicius *et al.,* "Nanohole plasmons in optically thin gold films," *J. Phys. Chem. B*, vol. 111, no. 3, pp. 1207–1212, Jan. 2007.

[18] J. Alegret, P. Johansson, and M. Käll, "Green's tensor calculations of plasmon resonances of single holes and hole pairs in thin gold films," *New J. Phys.*, vol. 10, no. 10, p. 105004, Oct. 2008.

[19] Y. Alaverdyan, B. Sepulveda, L. Eurenius, E. Olsson, and M. Käll, "Optical antennas based on coupled nanoholes in thin metal films," *Nat. Phys.*, vol. 3, no. 12, pp. 884–889, Dec. 2007.

[20] Y. Alaverdyan, E. M. Hempe, A. N. Vamivakas, E. Haibo, S. A. Maier, and M. Atatüre, "Spectral and angular distribution of Rayleigh scattering from plasmon-coupled nanohole chains," *Appl. Phys. Lett.*, vol. 94, no. 2, pp. 021112-1–021112-3, Jan. 2009.

[21] J. Yang *et al.,* "Broadband surface plasmon polariton directional coupling via asymmetric optical slot nanoantenna pair," *Nano Lett.*, vol. 14, no. 2, pp. 704–709, Feb. 2014.

[22] M. Janipour, T. Pakizeh, and F. Hodjat-Kashani, "Strong optical interaction of two adjacent rectangular nanoholes in a gold film," *Opt. Exp.*, vol. 21, no. 26, pp. 31 769–31 781, Dec. 2013.

[23] H. A. Bethe, "Theory of diffraction by small holes," *Phys. Rev.*, vol. 66, no. 7/8, pp. 163–182, Oct. 1944.

[24] R. Collin, *Field Theory of Guided Waves*. Piscataway, NJ, USA: IEEE Press, 1991.

[25] F. J. Garcia de Abajo, "Light transmission through a single cylindrical hole in a metallic film," *Opt. Exp.*, vol. 10, no. 25, pp. 1475–1484, Dec. 2002.

[26] B. Sepúlveda, Y. Alaverdyan, J. Alegret, M. Käll, and P. Johansson, "Shape effects in the localized surface plasmon resonance of single nanoholes in thin metal films," *Opt. Exp.*, vol. 16, no. 8, pp. 5609–5616, Apr. 2008.

[27] L. Yin *et al.,* "Surface plasmons at single nanoholes in Au films," *Appl. Phys. Lett.*, vol. 85, no. 3, pp. 467–469, Jul. 2004.

[28] S. H. Chang, S. Gray, and G. Schatz, "Surface plasmon generation and light transmission by isolated nanoholes and arrays of nanoholes in thin metal films," *Opt. Exp.*, vol. 13, no. 8, pp. 3150–3165, Apr. 2005.

[29] L. Tsang, J. A. Kong, K. H. Ding, and C. O. Ao, *Scattering of Electromagnetic Waves*. Hoboken, NJ, USA: Wiley, 2001.

[30] C. F. Bohren and D. R. Huffman, *Absorption and Scattering of Light by Small Particles*. Hoboken, NJ, USA: Wiley, 1983.

[31] A. Taflove and S. C. Hagness, *Computational Electrodynamics: The Finite-Difference Time-Domain Method*. Norwood, MA, USA: Artech House, 2005.

[32] T. Pakizeh, "Optical absorption of plasmonic nanoparticles in presence of a local interband transition," *J. Phys. Chem. C*, vol. 115, no. 44, pp. 21 826–21 831, Nov. 2011.

[33] J. P. B. Mueller and F. Capasso, "Asymmetric surface plasmon polariton emission by a dipole emitter near a metal surface," *Phys. Rev. B, Condens. Matter*, vol. 88, no. 12, pp. 121410-1–121410-6, Sep. 2013.

[34] N. Rotenberg *et al.,* "Plasmon scattering from single subwavelength holes," *Phys. Rev. Lett.*, vol. 108, no. 12, pp. 127402-1–127402-5, Mar. 2012.

[35] N. Rotenberg *et al.,* "Magnetic and electric response of single subwavelength holes," *Phys. Rev. B, Condens. Matter*, vol. 88, no. 24, pp. 241408-1–241408-5, Dec. 2013.

[36] H. Gao, J. Henzie, and T. W. Odom, "Direct evidence for surface plasmon-mediated enhanced light transmission through metallic nanohole arrays," *Nano Lett.*, vol. 6, no. 9, pp. 2104–2108, Sep. 2006.
[37] P. Johansson, "Electromagnetic Green's function for layered systems: Applications to nanohole interactions in thin metal films," *Phys. Rev. B, Condens. Matter*, vol. 83, no. 19, pp. 195408-1–195408-14, May 2011.
[38] J. D. Kraus and R. J. Marhefka, *Antennas for All Applications*, 3rd ed. New York, NY, USA: McGraw-Hill, 2003.